Chinese Chemical Letters 35 (2024) 109116

Contents lists available at ScienceDirect

Chinese Chemical Letters

journal homepage: www.elsevier.com/locate/cclet

First-principles study of the relationship between the formation of single atom catalysts and lattice thermal conductivity

Chaozheng He[a], Pei Shi[b], Donglin Pang[b], Zhanying Zhang[b], Long Lin[b,c,*], Yingchun Ding[d,**]

[a] Department of Chemistry and Chemical Engineering, Liaocheng University, Liaocheng 252059, China
[b] Henan Key Laboratory of Materials on Deep-Earth Engineering, School of Materials Science and Engineering, Henan Polytechnic University, Jiaozuo 454000, China
[c] School of Materials Science and Engineering, Henan Polytechnic University, Jiaozuo 454000, China
[d] Department of Basic Medicine, North Sichuan Medical College, Nanchong 637000, China

ARTICLE INFO

Article history:
Received 9 July 2022
Revised 17 September 2023
Accepted 17 September 2023
Available online 19 September 2023

Keywords:
First-principles calculation
Thermal conductivity
Single atom catalysts
Graphene
BN

ABSTRACT

Single atom catalysts (SACs) have been in the forefront of catalysts research because of their high efficiency and low cost and provide new ideas for development of renewable energy conversion and storage technologies. However, the relationship between the intrinsic properties of materials such as lattice thermal conductivity and catalysis remains to be explored. In this work, the lattice thermal conductivity of BN and graphene was calculated by ShengBTE. In addition, the adsorption properties of 3d-TM (TM = V, Cr, Mn, Fe, Co, Ni) on BN and graphene were investigated using first-principles methods, and it was found that Ni atom can form relatively stable SACs compared to other TMs. The molecular dynamics (MD) simulation and migration barrier of Ni loaded on BN and graphene were calculated. Our study found that graphene has higher thermal conductivity and is easier to form SACs than BN, but the SACs formed on BN surface have higher thermodynamic stability.

Single atom catalysts (SACs) with metal atoms dispersed on the support have been at the forefront of electrocatalytic reaction research because of their high selectivity and high utilization rate [1–5]. SACs can not only reduce the utilization cost of noble metal catalysts, but also interact with substrate, and then the interaction effect may lead to more favorable catalytic activity. So far, a large number of SACs have been synthesized experimentally [6–10] and widely used in many fields, such as CO_2 reduction reaction [11–13], CO oxidation reaction [14], water splitting [15,16], nitrogen reduction reaction (NRR) [17–19] and nitrogen oxide reduction reaction [20]. Zhao *et al.* synthesized Fe single atom supported on lignocellulose-derived carbon using Fe-$(O\text{-}C_2)_4$ as the active site of NRR [7]. Liu and his collaborators reported that the single Ag site of Ag-N_4 coordination and the single Fe site of Fe-N_4 coordination performed excellently in NRR, which were verified experimentally and theoretically [8,9]. Based on density functional theory (DFT), Fu *et al.* investigated that different single transition metals (TMs) (including Ti, V, Cr and Mn) embedded in the graphyne system for the highly selective reduction reaction of CO_2 to CH_4, and explored the relationship between the CO_2 reduction efficiency of each TM and corresponding reaction intermediates. The results show that Cr atom embedded in graphyne is not only the most effective choice for CO_2 reduction, but also can effectively inhibit hydrogen evolution reaction (HER) [11]. By means of DFT, Wu *et al.* found that graphyne is an excellent substrate for preparing single Fe atom catalysts, the adsorption properties of CO and O_2 on Fe-graphyne single atom catalyst was studied and simulated the CO oxide mechanism. The result show that the single Fe atom loaded on the graphyne has excellent catalytic activity for CO oxidation. It has potential application value to solve the increasingly serious environmental problems caused by CO emission and CO pollution [14]. Zhao and his co-workers systematically studied the capacity of NRR supported by a single TM atoms (Sc-Zn, Mo, Ru, Rh, Pd, Ag) on the defective monolayer BN, and the results show that defective BN supported single Mo atom performed the highest catalytic activity for nitrogen fixation through enzymatic mechanism, with an extremely low overpotential of 0.19 V [17]. Wu and his team systematically investigated the NO electrocatalytic reduction (NOER) performance for a series of TM atoms loaded on g-C_3N_4 using first principles calculation methods, and ascertained that the

* Corresponding author at: Henan Key Laboratory of Materials on Deep-Earth Engineering, School of Materials Science and Engineering, Henan Polytechnic University, Jiaozuo 454000, China.
** Corresponding author.
E-mail addresses: linlong@hpu.edu.cn (L. Lin), dyccqzx@163.com (Y. Ding).

https://doi.org/10.1016/j.cclet.2023.109116
1001-8417/

single Cu modified g-C_3N_4 (Cu@g-C_3N_4) was the most potential candidate material for NOER with excellent catalytic activity. It has a low limit potential with 0.371 V and high stability [20].

It can be seen from the above description that there are many studies on the synthesis of SACs on two-dimensional (2D) materials due to the unique optical, electronic, and mechanical properties of 2D materials compared to the bulk materials [21]. Since the emerge of graphene in 2004, 2D materials have gradually enter people's field of vision. More 2D materials have been synthesized experimentally and studied theoretically [22–29], such as h-BN [22,23], BC_3 [24,25], NC_3 [26,27]. Graphene is considered as one of the promising materials that can greatly improve the performance of many products due to its excellent properties and is currently one of the most widely studied materials [30–34]. H. Johll and H. C. Kang explored the adsorption properties of Fe, Co, Ni atoms on graphene [30]. Kim *et al.* used DFT to study the optical properties of graphene quantum dot systems with sizes of 0.4–1.1 nm and five TMs (Cr, Mo, Pd, Pt, and W), including the energy level of the highest occupied molecular orbital (HOMO) and lowest unoccupied molecular orbital (LUMO), adsorption spectra, zero-field splitting and intersystem-crossing gaps [31]. The electronic and magnetic properties of graphene and graphene nanoribbons have been studied theoretically by S. Ciraci *et al.* [32]. They also studied the binding energy, and electronic and magnetic properties of TM atoms adsorbed on one and both sides of graphene. In addition, BN has attracted much attention because of its chemical inertness, large indirect band gap and simple atomic structure. Moreover, monolayer BN has high chemical and thermal stability. Ma *et al.* conducted a detailed study that single Fe atom adsorbed on the monolayer BN performed the CO catalytic oxidation at room temperature, and the results showed that the catalytic activity of BN on CO oxidation was enhanced after adsorption of Fe atom [35]. Zheng and his co-worker system systematically studied the adsorption of TM atoms on monolayer BN by first principles calculation, and analyzed adsorption energy, charge density, magnetic moment and so on. This provides ideas for the application of spintronics and the development of magnetic nanostructures [36]. Smith *et al.* used first-principles calculation to study the electrocatalytic reduction of CO_2 to methane by a single TM loaded with defective monolayer BN, and the results showed that Fe and Co atom loaded on the BN not only have excellent catalytic activity for the electrocatalytic reduction of CO_2, but also was the most cost-effective electrocatalyst [37].

In addition, the importance of thermal properties of materials is gradually increasing in recent years. Heat dissipation is crucial for the performance, reliability, life and safety of electronic and optoelectronic devices, lithium-ion batteries, micro machines and other products. Due to the decrease of the size of electronic devices and the increase of dissipated power density in reduce circuits, heat dissipation is becoming a critical issue for the sustainable development of electronic industry. The diamond is the best bulk thermal conductor by previous studies, while Balandin *et al.* mentioned in study on the thermal performance of graphene and nanostructured carbon materials that carbon materials occupy the unique position on thermal performance through form a variety of allotropes, and the thermal conductivity of carbon nanotubes exceed diamond at room temperature [38]. Furthermore, the extremely high thermal conductivity of graphene indicates that its thermal conductivity is better than nanotubes [39]. Cai *et al.* also reported that the thermal conductivity of monolayer BN is 751 W m^{-1} K^{-1} at room temperature and found that the value of thermal conductivity of BN with thinner atomic thickness decrease with increasing thickness [40].

At present, research on SACs has been very common, but the relationship between catalysis and thermal conductivity of materials still need to explore. Both BN and graphene have similar structures due to their six-membered ring structure, and BN has thermal conductivity and mechanical strength comparable to graphene. Therefore, we systematically studied the relationship between the lattice thermal conductivity of BN and graphene and the formation of SACs in this work. We first calculated the lattice thermal conductivity of BN and graphene at different temperature through ShengBTE code, and found the lattice thermal conductivity of graphene is much large than of BN and the trend of decrease is larger with increase of temperature. Based on DFT, the adsorption properties of 3d-TM on the two surfaces were explored, respectively, and the molecular dynamic (MD) and migration barrier calculation were carried out with Ni atom loaded as an example. The results show that graphene with larger lattice thermal conductivity is more likely to form SACs than BN with smaller lattice thermal conductivity, but SACs on BN surface has higher thermodynamic stability. These results provide a strategy for designing SACs with low cost, high selectivity, and high catalytic activity.

In this work, the spin density functional theory is implemented by using the Vienna Ab initio Simulation Package (VASP) [41]. Projection enhanced wave (PAW) method is used to describe the interaction between ions and electrons [42]. The generalized gradient approximation (GGA) of Perdew-Burke Enzerhor (PBE) functional is used to describe the exchange correlation [43]. A $4 \times 4 \times 1$ BN supercell (containing 16 B atoms and 16 N atoms) and graphene supercell (containing 32 C atoms) was used for calculation. The cutoff energy was set at 500 eV. The vacuum layer was set at 20 Å to avoid periodic repetition effects. The Brillouin zone was sampled using a $5 \times 5 \times 1$ k-point grid mesh centered for geometry optimization. All structures were relaxed by using energy convergence criteria of 1.0×10^{-6} eV/atom and force convergence criteria of 0.01 eV/Å.

The adsorption energy (E_{ads}) [34–47] was calculated according to Eq. 1:

$$E_{ads} = E_{total} - E_{surface} - E_{TM} \quad (1)$$

where E_{total}, $E_{surface}$ and E_{TM} are energy of graphene or BN and adsorbates, pristine graphene or BN, TM atoms, respectively.

The cohesive energy (E_{coh}) [48] was calculated according to Eq. 2:

$$E_{coh} = E_{bulk}/n - E_{atom} \quad (2)$$

where E_{bulk} is the energy of the unit cell of a metal crystal and n is the number of metal crystal. E_{atom} is the energy of an atom in a cell.

Quantum ESPRESSO (QE) code was used to calculate the second-order and third-order force constants, and ShengBTE code was used to solve the phonon and electron Boltzmann transport equation (BTE), so as to obtain the lattice thermal conductivity of BN and graphene [49–51]. The second-order force constants are calculated using density functional perturbation theory (DFPT) by VASP and Phonopy package [52–54]. To accurately calculate phonon frequencies, BN and graphene use $4 \times 4 \times 1$ and $5 \times 5 \times 1$ grids, respectively. The Third-order force constant is calculated by VASP and Thirdorder software package.

As shown in Figs. 1a and b, we constructed $4 \times 4 \times 1$ BN and $5 \times 5 \times 1$ graphene optimized supercell geometric structure, and labeled the adsorption sites of TMs on their surfaces. In Fig. 1a, T_B and T_N represent the top position of B atom and the top position of N atom on BN, Bri represents the top position of B-N bond, and H represents the hole of a hexatomic ring consisting of three B atoms and three N atoms. In Fig. 1c, T_C represents the top position of C atom on graphene, Bri represents the top of C-C bond, and H represents the hole of a hexatomic ring consisting of 6 C atoms. The optimized lattice parameter of BN is 10.05 Å, and that of graphene is 9.84 Å. Phonon dispersion effects of BN and graphene were cal-

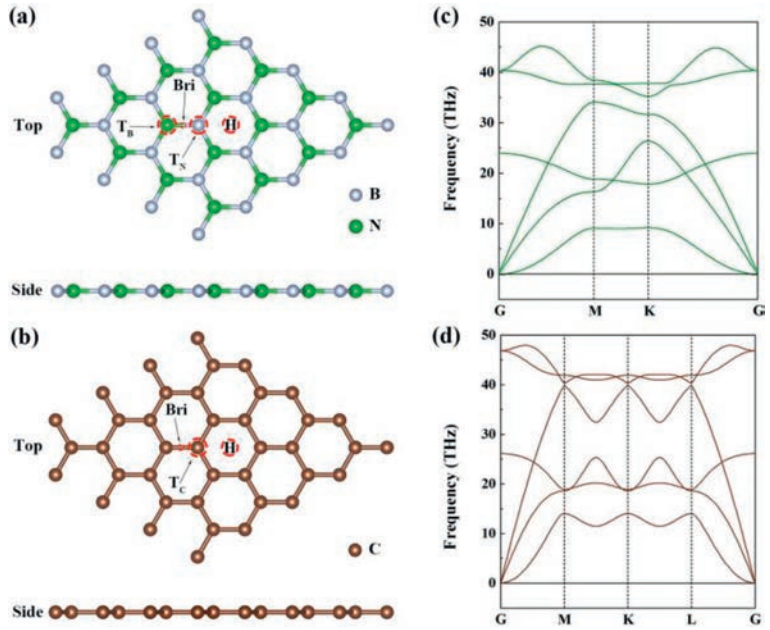

Fig. 1. Optimized geometrical structures of BN (a) and graphene (b), respectively. (c, d) Phonon dispersion of BN and graphene, respectively.

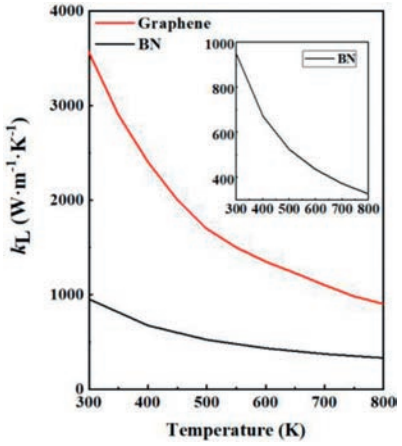

Fig. 2. The lattice thermal conductivity of BN and graphene.

culated by using DFPT as shown in Figs. 1c and d. It can be seen that phonon frequencies of BN and graphene have no negative and virtual frequency in the whole of Brillouin zone, indicating dynamical stability of both the structures.

The lattice thermal conductivity is calculated by solving phonon and electron BTE using VASP in conjunction with the ShengBTE package. In this work, we calculated the lattice thermal conductivity of BN and graphene at 300–800 K and shown in Fig. 2, the specific thermal conductivity is shown in Table S1 (Supporting information). At 300 K, the lattice thermal conductivity of graphene is 3550 W m^{-1} K^{-1}, while that of BN is only 950 W m^{-1} K^{-1}. It is clear that the lattice thermal conductivity of graphene is much larger than that of BN. The calculation results in Fig. 2 and Table S1 show that the lattice thermal conductivity decrease gradually with the increase of temperature, and the decrease trend of graphene is more obvious.

The adsorption of 3d-TMs (V, Cr, Mn, Fe, Co, and Ni) on BN and graphene surfaces was calculated. TM atoms on SACs can not only provide unoccupied d orbitals to accept lone pair electrons from gas molecular, but also feedback electrons to antibonding orbitals of gas molecular. The initial TM elements of 3d-TM, such as Sc and Ti, contribute most of the electrons in the d orbital to the substrate in order to exist stably on the substrate. On the other hand, the late TMs (Cu and Zn) of 3d-TM have no unoccupied d orbital to accept the lone pair electrons of the gas molecules. All these cases may lead to weak binding strength between TM atom and gas molecular, and weak binding will lead to lower activity in the subsequent catalytic reactions. Therefore, 3d-TMs Sc, Ti, Cu and Zn are not studied here. Figs. 3a and b show the adsorption energy (E_{ads}) and charge transfer (ΔQ) of TMs at different sites on BN and graphene surface, and the specific values are shown in Tables S2 and S3 (Supporting information), respectively. The histogram corresponds to the E_{ads} on the left ordinate, while the line graph corresponds to the ΔQ on the right ordinate. The negative values of E_{ads} for all structures indicate that all TM atoms can spontaneously and stably anchor to BN and graphene surfaces. The E_{ads} of a single TM atom on the graphene surface is slightly larger than that on the BN surface. Combined with the above thermal conductivity calculation, we speculate that graphene with higher thermal conductivity has stronger interaction with 3d-TM than BN and is more likely to form SACs. Taking Ni loaded on BN and graphene, respectively, as an example, Figs. 3c and d show the optimized structure.

The cohesive energy (E_{coh}) of metal is widely defined as the energy required for metal crystal cells to decompose into isolated single atoms, and some researchers have found a relationship between the growth form of TM on surface and the ratio of adsorption energy and cohesive (E_{ads}/E_{coh}) [55–58]. In order to understand whether TM atoms are more likely to form monatomic catalysts on BN and graphene surfaces or more likely to aggregate into metal clusters, we compared the adsorption energy and cohesive energy (E_{ads}/E_{coh}). Generally, if the ratio is small, it indicates that TM is easier to aggregate and grow into three-dimensional (3D) clusters, on the contrary, a large ratio indicates that 2D growth is easier to achieve and SACs is easier to form. We calculated the values of E_{ads}/E_{coh} for all structures on BN and graphene and listed them in Tables S2 and S3. In addition, the ratio of TM loads on the graphene surface is generally slightly larger than that on BN. Therefore, we believe that TM atoms can be stably anchored on BN and graphene surfaces, and TM is more likely to form SACs on graphene surfaces than BN. Combined with the previous calculation results of thermal conductivity, we think that 2D materials

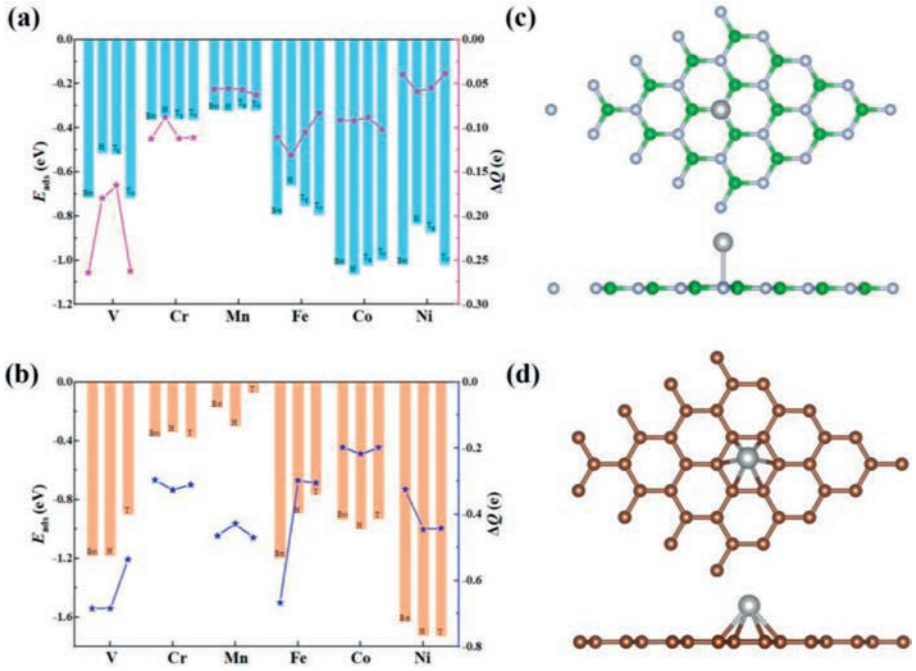

Fig. 3. (a, b) The adsorption energy of single TM atom at different sites on BN and graphene surface and the corresponding number of TM atom charge transfer, respectively. (c, d) The optimized structures of Ni atom loaded at the N-atom top of BN and the hollow on graphene surface, respectively.

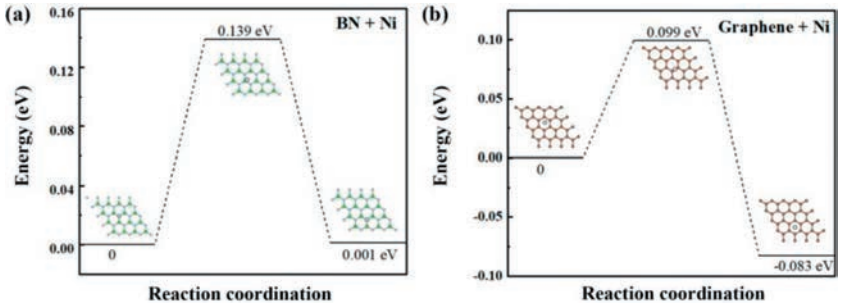

Fig. 4. The migration barrier for the adsorbed Ni atom from the anchored site to a neighboring site. (a) Ni loaded the BN surface. (b) Ni loaded the graphene surface.

with high thermal conductivity may be more likely to form SACs for a series of reactions.

It can be seen from Tables S2 and S3 that the maximum ratio in our calculation results is 0.181 on BN and 0.306 on graphene when Ni atoms are loaded on the surface. Therefore, we take the example of Ni atoms anchoring on BN and graphene surfaces in the following work to study their thermodynamic stability through MD and calculate the migration barrier of Ni atoms on the surfaces by searching transition states.

In addition, we simulated the thermal stability of Ni atom loaded BN and graphene surface at 800 K by first-principles MD, in which the time step was set at 2.0 fs for a total period of 10 ps. In the MD simulation of BN, there is no obvious geometric deformation and no Ni atom migration on the surface, as shown in Fig. S1 (Supporting information). The large adsorption energy and good thermal stability indicate that the top position of N atom on BN can be used as a good anchor site for single Ni atom and has high stability. In MD simulation of graphene, although there is no obvious geometric deformation, Ni atoms are not stable at the active site, indicating that Ni atoms are easy to migrate at the surface. Combined with the above calculation of the thermal conductivity of BN and graphene, it can be seen that the stability of the SACs formed by graphene with higher thermal conductivity as a substrate is not as good as that formed by BN. For this reason, we calculated the migration barrier of Ni atom adsorbing from the top of N atom to the adjacent top of N atom on BN surface and the migration barrier of Ni atom adsorbing from vacancy to adjacent vacancy on graphene surface. As can be seen from Fig. 4, the migration barrier of Ni atom on BN surface is 0.139 eV, while that on graphene surface is 0.099 eV. Although the migration barrier is small, the Ni atom is still larger on BN surface than on graphene surface. In a word, combined with the MD simulation, we can conclude that the Ni atom is more stable on BN surface anchoring than on graphene surface.

To summarize, by means of first-principles calculation, we first studied the phonon dispersion of monolayer BN and graphene using density functional perturbation theory, and found that both have good dynamic stability. Secondly, the ShengBTE program was used to calculated the lattice thermal conductivity of BN and graphene. The results show that graphene has a larger lattice thermal conductivity than BN, and the lattice thermal conductivity decreases with the increase of temperature. Then, the adsorption properties of 3d-TM atoms on BN and graphene surfaces were studied, and by combining thermal conductivity, we guessed that 2D materials with higher thermal conductivity were more likely to form monatomic catalysts. Finally, the MD simulation was carried out and the migration barrier was calculated by taking Ni atom loaded on the surface as an example. The above results show that

graphene has high thermal conductivity and is easier to form single atom catalysts, but the monatomic catalyst formed on BN surface has better thermodynamic stability.

Declaration of competing interest

The authors declare that they have no known competing financial interests or personal relationships that could have appeared to influence the work reported in this paper.

Acknowledgments

This work was supported by the Key Projects of NSFC-Henan Joint Fund (Nos. U1404216 and U2004209), the Natural Science Foundation of China (No. 21603109), the Scientific Research Program Funded by Shaanxi Provincial Education Department (No. 20JK0676), the Fundamental Research Funds for the University of Henan Province (No. 200303), and Dalian High-level Talent Innovation Support Program (No. 2019RQ075).

Supplementary materials

Supplementary material associated with this article can be found, in the online version, at doi:10.1016/j.cclet.2023.109116.

References

[1] S.K. Iyempereumal, T.D. Pham, N.A. Deskins, et al., J. Phys. Chem. C 122 (2018) 25274–25289.
[2] Y. Wang, Y. Du, Y. Meng, et al., Appl. Surf. Sci. 563 (2021) 150277.
[3] H. Jing, P. Zhu, X. Zheng, et al., Adv. Powder Mater. 1 (2022) 100013.
[4] Q. Wang, Q. Feng, Y. Lei, et al., Nat. Commun. 13 (2022) 3689.
[5] T. Cui, Y. Wang, Y. Lei, et al., Angew. Chem. Int. Ed. 61 (2022) e202115219.
[6] L. Chen, C. He, Y. Lei, et al., Chin. Chem. Lett. 32 (2021) 53–56.
[7] H. Zhao, S. Zhang, M. Jin, et al., Angew. Chem. Int. Ed. 59 (2020) 13423–13429.
[8] Y. Chen, X. Liu, J. Luo, et al., ACS Nano 14 (2020) 6938–6946.
[9] F. Lv, J. Luo, X. Liu, et al., Nano Energy 61 (2019) 420–427.
[10] S. Jian, Z. Tian, J. Hu, et al., Adv. Powder Mater. 1 (2022) 100004.
[11] L. Fu, R. Wang, C. He, et al., Chem. Eng. J. 414 (2021) 128857.
[12] J. Chen, Z. Wang, H. Lee, et al., Mater. Today Phys. 12 (2020) 100176.
[13] X. Sun, L. Sun, Y. Lei, et al., Angew. Chem. Int. Ed. 61 (2022) e202207677.
[14] P. Wu, P. Du, C. Cai, et al., Phys. Chem. Chem. Phys. 17 (2015) 1441–1449.
[15] X.H. Chen, Q. Zhang, L.L. Wu, et al., Mater. Today Phys. 15 (2020) 100268.
[16] M. Ma, L. Chen, J. Zhao, et al., Chin. Chem. Lett. 30 (2019) 2191–2195.
[17] J. Zhao, Z. Chen, J. Am. Chem. Soc. 139 (2017) 12480–12487.
[18] W. Song, L. Fu, C. He, et al., Adv. Theory Simul. 4 (2021) 21000044.
[19] R. Wang, C. He, W. Chen, et al., Chin. Chem. Lett. 32 (2021) 3821–3824.
[20] Q. Wu, W. Wei, Y. Dai, et al., J. Phys. Chem. C 123 (2019) 31043–31049.
[21] J. Yu, C. He, L. Yu, et al., Chin. Chem. Lett. 32 (2021) 3149–3154.
[22] Z. Ma, Z. Cui, R. Sa, et al., Nanoscale 12 (2020) 1541–1550.
[23] I. Jo, M.T. Pettes, L. Shi, et al., Nano Lett. 13 (2020) 550–554.
[24] H. Tanaka, Y. Kawamata, H. Yanagisawa, et al., Solid State Commun. 136 (2005) 22–25.
[25] Q. Wang, L. Chen, Phys. Rev. B 54 (1996) 4.
[26] Q. Hu, Q. Wu, H. Wang, Phys. Status Solidi B 249 (2012) 784–788.
[27] C.H. Lee, D. Zhang, Y.K. Yap, J. Phys. Chem. C 116 (2012) 1798–1804.
[28] Y. Liu, L. Chen, X. Liu, et al., Chin. Chem. Lett. 33 (2022) 1385–1389.
[29] H. Ji, J. Ni, D. Zhao, W. Liu, ACS EST Eng. 2 (2022) 1015–1038.
[30] H. Johll, H.C. Kang, Phys. Rev. B 79 (2009) 245416.
[31] D.H. Kim, A.H. Kulahlioglu, B.D. Kong, et al., J. Mater. Chem. C 9 (2021) 12550–12558.
[32] H. Sevincli, M. Topsakal, S. Ciraci, et al., Phys. Rev. B 77 (2008) 195434.
[33] X. Jiang, L. Zhang, H. Liu, et al., Angew. Chem. Int. Ed. 60 (2021) 21751–21755.
[34] L. Zhang, X. Jiang, Z. Zhong, et al., Angew. Chem. Int. Ed. 59 (2020) 23112–23116.
[35] C. Ma, B. Liu, S. Yan, Mol. Catal. 495 (2020) 111165.
[36] S. Li, F. Zheng, P. Zhang, et al., J. Appl. Phys. 123 (2018) 095110.
[37] X. Tan, H.A. Tahini, S.C. Smith, et al., Adv. Theory Simul. 2 (2018) 1800094.
[38] A.A. Balandin, Nat. Mater. 10 (2011) 569–581.
[39] A.A. Balandin, S. Ghosh, W. Bao, et al., Nano Lett. 8 (2008) 902–907.
[40] Q. Cai, D. Scullion, E.J.G. Santos, et al., Sci. Adv. 5 (2019) eaav0129.
[41] M.C. Wasson, X. Zhang, K.I. Otake, Chem. Mater. 32 (2020) 8522–8529.
[42] P.E. Blöchl, Phys. Rev. B 50 (1994) 17953–17979.
[43] J.P. Perdew, Y. Wang, Phys. Rev. B 45 (1992) 13244–13249.
[44] C. He, R. Wang, H. Yang, S. Li, L. Fu, Appl. Surf. Sci. 507 (2020) 145076.
[45] R. Sun, C. He, L. Fu, et al., Chin. Chem. Lett. 33 (2022) 527–532.
[46] W. Song, K. Xie, C. He, et al., Phys. Chem. Chem. Phys. 23 (2021) 10418.
[47] X. Fu, H. Yang, L. Fu, et al., Chin. Chem. Lett. 32 (2021) 1089–1094.
[48] H. Yang, C. He, L. Fu, et al., Chin. Chem. Lett. 32 (2021) 3202–3206.
[49] E. Jossou, L. Malakkal, B. Szpunar, et al., J. Nucl. Mater. 490 (2017) 41–48.
[50] B. Szpunar, J.I. Ranasinghe, L. Malakkal, J.A. Szpunar, J. Alloy. Compd. 879 (2021) 160467.
[51] B. Roondhe, V. Sharma, T.S. Dasgupta, et al., Appl. Surf. Sci. 533 (2020) 147513.
[52] Y. Cai, L. Zeng, Y. Zhang, X. Xu, Phys. Chem. Chem. Phys. 20 (2018) 20726–20731.
[53] B. Szpunar, J.I. Ranasinghe, L. Malakkal, J.A. Szpunar, J. Phys. Chem. Solids 146 (2020) 109636.
[54] S. Illera, M. Pruneda, L. Colombo, P. Ordejón, Phys. Rev. Mater. 1 (2017) 044006.
[55] L. Hu, X. Hu, X. Wu, J. Deng, Phys. B 405 (2010) 3337–3341.
[56] X. Liu, C.Z. Wang, M. Hupalo, et al., Phys. Chem. Chem. Phys. 14 (2012) 9157–9166.
[57] M. Manadé, F. Viñes, F. Illas, Carbon 95 (2015) 525–534.
[58] T. Hu, J. Hong, J. Phys. Chem. C 119 (2015) 8199–8207.